Structural and dielectric properties of laser ablated $BaTiO_3$ films deposited over electrophoretically dispersed $CoFe_2O_4$ grains

J. G. Barbosa[1], I.T. Gomes[1,2], M.R. Pereira[1], C.Moura[1], J.A. Mendes[1], and B.G. Almeida[1*]

[1]Centro de Física, Universidade do Minho, Campus de Gualtar, 4710-057 Braga, Portugal

[2]Departamento de Física and IFIMUP-IN, Institute of Nanoscience and Nanotechnology, Universidade do Porto, Rua do Campo Alegre 687, 4169-007 Porto, Portugal

Abstract

Thin film nanocomposites with mixed connectivity, composed by $CoFe_2O_4$ grains deposited by electrophoresis on Si|Pt substrates and subsequently covered by a laser ablation deposited $BaTiO_3$ layer were prepared with different cobalt ferrite concentrations. Their structure presented a combination of $BaTiO_3$, with its tetragonal and the orthorhombic phases coexisting at room temperature, and $CoFe_2O_4$ with the cubic spinel structure. The cobalt ferrite nanograins were under in-plane tensile stress, while the $BaTiO_3$ phase was under in-plane compressive stress. The dielectric measurements showed that as the barium titanate grain size decreased, its ferroelectric Curie temperature shifted to lower temperatures relative to the bulk. This grain size dependent T_C shift was associated and modeled by a core-shell structure of $BaTiO_3$ grains in the films, with a tetragonal core and cubic shell. Additionally a diffuse tetragonal-orthorhombic phase transition was observed and, in agreement with Raman spectroscopy results, associated to the coexistence of barium titanate orthorhombic and tetragonal phases in the room temperature region. This led to the formation of polar nanoclusters with random polarization orientations, which induced a frustrated phase transition between the tetragonal and orthorhombic phases of barium titanate in the films.

Keywords: $BaTiO_3$-$CoFe_2O_4$, Multiferroic Composite, Mixed Connectivity, Structural Properties, Dielectric Properties

*Corresponding author: bernardo@fisica.uminho.pt, tel: +351253604063, fax: +351253604079

1. Introduction

In recent years, the synthesis of materials that exhibit simultaneous ferromagnetic and ferroelectric characteristics has been attracting much scientific and technological interest. In these multiferroic materials, the coupling between the magnetic and electric degrees of freedom, the so-called magnetoelectric effect, may give rise to new physical phenomena and applications [1-6]. In multiferroic composite structures, composed by ferroelectric (piezoelectric) and ferromagnetic (magnetostrictive) materials, the elastic interactions between the piezoelectric and magnetostrictive phases induce a magnetoelectric behavior. In thin film form, three main phase mixing geometries have been developed for these composites, namely, magnetic grains in a piezoelectric matrix (0-3 connectivity), multilayer structures (2-2 connectivity) and magnetostrictve pillars inside a piezoelectric matrix (1-3 connectivity) [7-9]. However, in the 2-2 geometries, i.e., horizontal multilayer structures, the clamping effect from the substrate limits the deformation of the phases, leading to a decreased stress mediated coupling between them [10]. Also for the 1-3 geometry, where magnetostrictive columns are dispersed on a piezoelectric matrix, the leakage current associated to magnetostrictive phase (normally metallic or ceramics with lower resistivity than the piezoelectric material) hinders the electrical polarization from the piezoelectric phase [2]. The same problem appears for 0-3 structures where magnetostrictive grains are dispersed in a piezoelectric matrix, when the magnetostrictive concentration exceeds the percolation limit.

In order to reduce these problems, a new type of structure has been proposed [11;12]. In this structure, magnetostrictive grains are dispersed on a substrate and subsequently covered by a piezoelectric film, filling the voids between them. The final structure can be considered as being constituted by mixed connectivity types: it consists on a 2-2 type structure composed by an upper piezoelectric layer and a bottom composite layer. The

composite layer itself can be considered as a 1-3 structure where the magnetostrictive grains are dispersed in the piezoelectric matrix. With this structure, it is expected that the interface area between the phases is increased relative to typical bilayer films. At the same time the 1-3 composite bottom layer helps to decrease the clamping effect of the substrate and the piezoelectric top layer limits conduction effects arising from the magnetostrictive phase.

For this type of mixed connectivity composites the $BaTiO_3$-$CoFe_2O_4$ combination has, up to now, been poorly explored. Here, two phase films composed by magnetostrictive cobalt ferrite ($CoFe_2O_4$) grains electrophoretically dispersed on $Si/SiO_2/Ti/Pt$ substrates and subsequently covered by a laser ablation deposited ferroelectric barium titanate ($BaTiO_3$) film were prepared, to form the mixed connectivity structure. Their structure and dielectric properties have been investigated.

In these nanostructures their properties and performance depend critically on the phase morphology and internal stresses distribution, as well as on the elastic phase/phase and phase/substrate interactions. In this respect, in thin film form, it is known that the $BaTiO_3$ phase diagram is highly dependent on mechanical stresses and grain sizes [13,14]. The relevance of mechanical stresses on the $BaTiO_3$ phase diagram has been shown for an epitaxial film, based on Landau-Devonshire phenomenological formalism, where in addition to significant shifts on phase transition temperatures relative to the bulk, the coexistence of phases at different temperatures has been predicted [14]. Experimentally it has long been observed the stabilization of the orthorhombic phase, coexisting with the tetragonal one, at room temperature, for ceramics with grain sizes below 500 nm [15,16].

Additionally, significant shifts on ferroelectric Curie temperatures have been observed and related with small grain sizes. For example, Curie temperatures of the order of 368 K (below the bulk value of 403 K [17]) have been reported for $BaTiO_3$ grains with 100 nm [18]. The decreasing grain size results in a decreasing of the $BaTiO_3$ tetragonality that disappears

below a certain critical size. This critical grain size for the stabilization of the ferroelectric phase on $BaTiO_3$ is still under investigation and sizes between 8 nm and 30 nm have been reported [16, 18-21]. Thus, here, in order to address these problems, the influence of the structural properties of the $BaTiO_3$-$CoFe_2O_4$ mixed connectivity composite nanostructures on their dielectric properties has been studied. The observed decrease of the barium titanate ferroelectric Curie temperature and the strong frequency dispersion of the dielectric permittivity near room temperature were correlated with the combination of reduced grain size and residual stresses in the films.

2. Experimental:

The nanogranular $(BaTiO_3)_{1-x}$ - $(CoFe_2O_4)_x$ films were deposited on $Si/SiO_2/Ti/Pt$ substrates. Initially, a water suspension of $CoFe_2O_4$ nanograins was obtained by a coprecipitation method [12], where $FeCl_3 \cdot 6H_2O$ and $CoCl_2 \cdot 6H_2O$ precursors were used and the reaction temperature was ~78ºC. The obtained water solution was then dried in order to obtain cobalt ferrite powder. Next, the powder was dispersed in 1-octanol with a concentration of 4.5 g/l. A small amount of iodine, with concentration of 1.6×10^{-2} M, was then added to the suspension in order to charge the $CoFe_2O_4$ grains. The formed suspension was ultrasonicated for 60 minutes. In order to deposit $CoFe_2O_4$ grains by EPD, two parallel electrodes were placed inside the suspension, separated by a distance of 15 mm. $Si/SiO_2/Ti/Pt$ substrates were used as cathodes (where the grains were deposited) while the anode was a $Si/SiO_2/TiO_2/Pt$ plate. The dc voltage applied between the electrodes during electrophoresis was 25 V and the deposition times were (in seconds): 150, 300, 600, 900, 1160 and 1870. The discontinuous films were then dried at the air, washed in distilled water to remove NaCl contamination and heated at 500ºC during 1 hour, in order to vaporize organic residues.

The dispersed cobalt ferrite grains in $Si/SiO_2/Ti/Pt$ were subsequently covered with a barium titanate layer. This layer was deposited by laser ablation with a KrF excimer laser (wavelength λ = 248 nm), at a fluence of 2 J/cm^2 and a 10 Hz repetition rate. The oxygen pressure was 0.8 mbar, the substrate temperature was ~625ºC and the distance between target and substrate was 4 cm. Prior to deposition, the films were kept at 500ºC during 1 hour in order to evaporate residuals from the sample surface. The structural studies were performed by X-ray diffraction (XRD) and were carried out with a Philips PW-1710 diffractometer using Cu Kα radiation. Raman studies were performed using a Jobin-Yvon T64000 spectrometer with an excitation wavelength at 514.5 nm, from an Ar laser. Scanning electron microscopy (SEM) and Energy dispersive X-ray spectroscopy (EDX) was performed with a Nova NanoSEM 200 microscope.

In order to perform the dielectric measurements the thin film samples were connected forming a parallel plate capacitor included in a LCR network. To form the capacitor, the substrate platinum layer was used as the bottom electrode while the top electrode was a small circular silver paste contact (air dried), glued on the film surface, with approximately 1 mm in diameter. The test samples had typical sizes of 5 mm in length and 5 mm wide. A Waine Kerr 6440A impedance analyzer together with a dedicated computer and software were used in order to acquire the data. Shielded test leads were employed to avoid parasitic impedances due to the connecting cables. The measurements were performed at a rate of 1ºC/min, using a Polymer Labs PL706 PID controller and furnace.

3. Results and discussion

3.1. Structure and microstructure

The preliminary structural properties have been previously characterized [12] and here we present the main results. The scanning electron microscopy (SEM) measurements revealed

that the samples are composed by $CoFe_2O_4$ grains dispersed on the substrate surface with the $BaTiO_3$ layer growing on top and filling the space between them. A columnar growth of the $BaTiO_3$ film is observed, with a $BaTiO_3$ layer thickness of around 1.12 μm, for all the samples.

X-ray diffraction measurements were performed on the nanocomposites with cobalt ferrite concentrations (x) in the range from x = 2% to x = 22% and their corresponding spectra are shown in Figure 1. The films are polycrystalline and composed by a mixture of $BaTiO_3$ and $CoFe_2O_4$. The cobalt ferrite grains have a cubic inverse spinel structure, indicated by the presence of their (311) peak that increases in intensity as the $CoFe_2O_4$ concentration increases in the films.

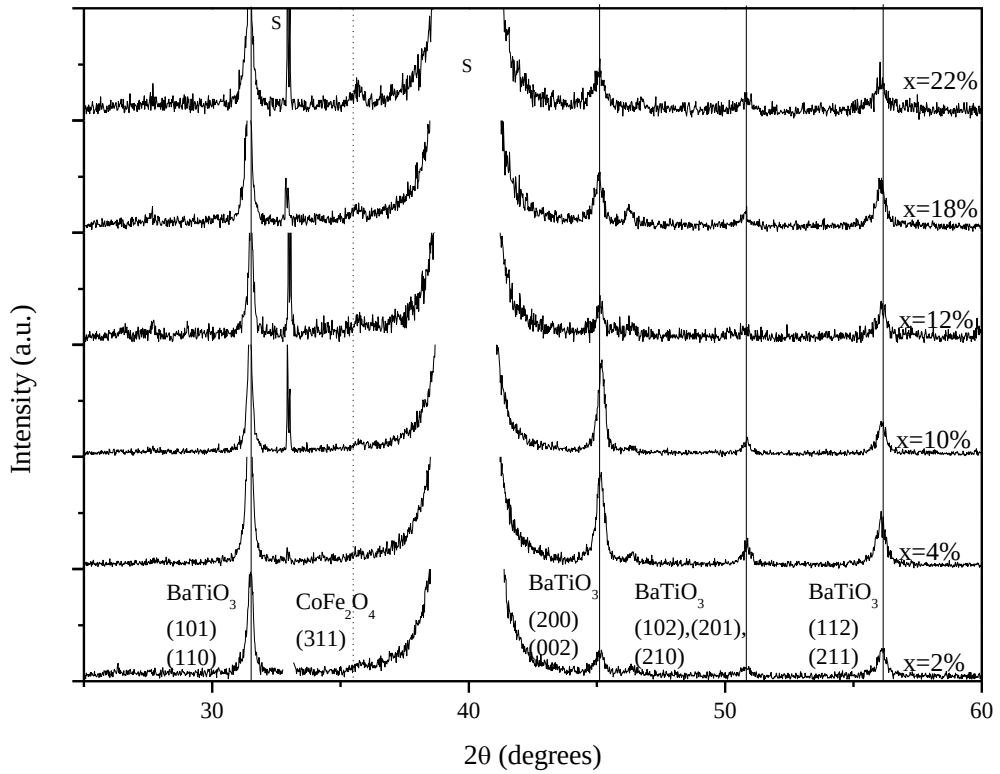

Figure 1: X-ray diffraction spectra of the samples deposited with cobalt ferrite concentrations in the range 2%-22%. The vertical lines mark the peak position of the bulk $CoFe_2O_4$ cubic spinel phase (…), and the tetragonal-$BaTiO_3$ phase (—). The peaks marked with an S are from the substrate.

In its bulk form, $BaTiO_3$ is cubic at high temperatures. At a temperature ~403 K it transforms from a cubic to a tetragonal structure that remains at room temperature [17].

Below ~278 K it changes to an orthorhombic structure and, finally, to a rhombohedral phase at ~193 K [17]. On $BaTiO_3$ nanograins, depending on grain sizes and stress conditions, the cubic, tetragonal and orthorhombic phases can be stabilized at room temperature [13, 14]. Here, in the XRD spectra it is possible to identify a broadening and an asymmetry of, for example, the (200) peaks, indicating the doubling of the peaks induced by the presence of a polar phase on the $BaTiO_3$ layer, at room temperature [12]. This was further confirmed by Raman spectroscopy measurements as will be discussed on the next section. The diffraction peaks were fitted with pseudo-Voigt functions in order to determine peak positions and widths.

The $BaTiO_3$ and $CoFe_2O_4$ grain sizes were determined from the (110) and (311) X-ray diffraction peaks widths, respectively, using the Scherrer equation [22]. Figure 2 shows the grain size of the barium titanate phase on the films, for different $CoFe_2O_4$ concentrations (x). The $BaTiO_3$ grain size initially rises from 41 nm, for x=2%, to a maximum of 45 nm, at x=12%, and then shows a tendency to decrease with increasing x until x=22% where the obtained grain size is 30 nm. This behavior can be ascribed to the increasing amount of nucleation centers for film growth, as the number of electrophoretic-deposited $CoFe_2O_4$ grains cover the substrate surface, before the $BaTiO_3$ layer deposition. On the other hand, the grain sizes of the $CoFe_2O_4$ phase on the films are around 20 nm and they are similar for different cobalt ferrite contents in the samples. This is due to the electrophoretic preparation step of this phase, which, except for the deposition time, was similar for the different samples.

Considering the room temperature tetragonal phase, the corresponding a and c $BaTiO_3$ lattice parameters are also represented on Figure 2. They were obtained from a fit to the (002) and (200) peak positions. In the films, the a lattice parameter is always above the bulk value ($a_{BaTiO3,bulk}$ = 3.994 Å [23]), while the c lattice parameter is always below the bulk one ($c_{BaTiO3,bulk}$ = 4.038 Å [23]). Thus, these lattice parameters indicate an expansion of the unit

cell along the *a* direction, compared to the bulk, and a contraction along the *c* direction. The reduction of the *c* lattice parameter and the expansion of the *a* parameter, relative to the tetragonal bulk form, and the consequent reduction of the cell distortion, can be explained in terms of the formation of a composite structure inside the $BaTiO_3$ grains [21,24,25], where the grains are composed by three layers: a tetragonal core, a gradient lattice strained layer and a surface cubic layer. Since the surface cubic layer thickness is approximately constant [25], the volume fraction of these phases depends on the grain size, with the gradient lattice strained layer and the surface cubic layer becoming important for small grain sizes. This then leads to a progressive decrease of *c* and an increase of *a*, that tends to suppress the tetragonal distortion and consequently the ferroelectricity, for sufficiently low grain sizes.

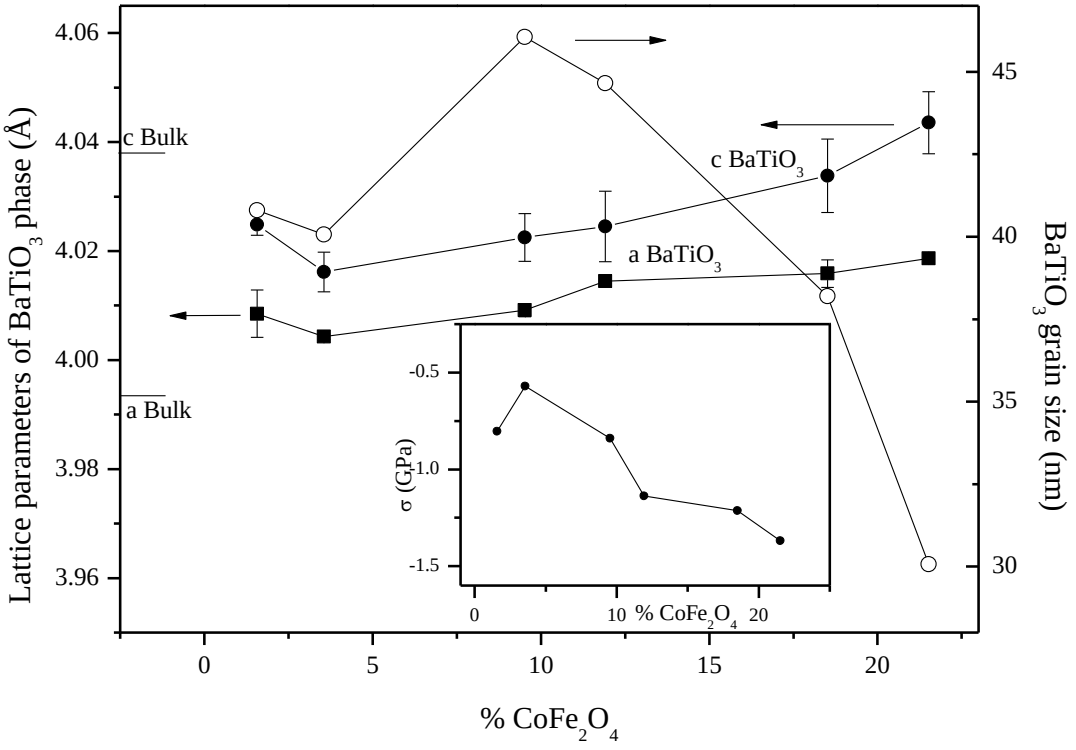

Figure 2: On the left axis the barium titanate lattice parameters, obtained from the XRD peaks (002) and (200), are shown as a function of cobalt ferrite content. On the right axis the $BaTiO_3$ grain size, obtained from the (110) peak width with the Sherrer equation, is plotted. The inset shows the in-plane biaxial stress on the $BaTiO_3$ grains, calculated from the (200) peak positions**.**

In the films, when the cobalt ferrite content increases, and after a slight decrease from *x*=2% to *x*=4%, there is an increase of both $BaTiO_3$ lattice parameters. Since the lattice parameters are obtained from interplanar distances between planes parallel to the sample surface, due to the measurement geometry of the θ-2θ X-ray diffraction scans, the increase of these two out-of-plane parameters results from the presence of in-plane compressive stresses on the $BaTiO_3$ grains. To estimate the in-plane strain, the in-plane stresses on grains with *a* axes perpendicular to surface were estimated by [26]:

$$\varepsilon_a = s_{11} \times \sigma_3 + s_{12} \times \sigma_1 + s_{13} \times \sigma_2 \qquad (1)$$

where s_{11}, s_{31} and s_{21} are the compliances, ε_a is the strain on the *a* axes and σ the stress. Assuming no stress out-of-plane ($\sigma_3 = 0$) and isotropic stress in plane ($\sigma_1 = \sigma_2 = \sigma$), equation 1 reduces to:

$$\varepsilon_a = (s_{12} + s_{13}) \times \sigma \qquad (2)$$

with s_{13}=-2.2×10^{-3} GPa^{-1}, s_{12}=-2.31×10^{-3} GPa^{-1} [27]. The in-plane stresses on $BaTiO_3$ grains, as a function of $CoFe_2O_4$ content, were estimated by equation 2 with ε_a determined from the *a* lattice parameter obtained from the (200) XRD peak, through $\varepsilon_a = (a_{BaTiO3,film} - a_{BaTiO3,bulk})/a_{BaTiO3,bulk}$. They are represented on the inset graphic on Figure 2 and the observed negative values indicate that the $BaTiO_3$ grains are under an in-plane compressive stress. After a slight decrease from *x*=2% to *x*=4%, the compressive stress increases, as the $CoFe_2O_4$ content increase, from σ = -0.6 GPa for x=4% to σ = -1.4 GPa for x=22%.

On the other hand, the lattice parameter of $CoFe_2O_4$, obtained from the (311) peak position and presented on the left axis of Figure 3, is always below the bulk value ($a_{CoFe2O4,bulk}$ = 8.387 Å [23]), changing from 8.31 Å to 8.34 Å when the $CoFe_2O_4$ increases from x = 2% to *x* = 22%, respectively. Thus, the cobalt ferrite phase is under a compressive strain in the direction perpendicular to the films surface, indicating the presence an in-plane tensile stress that progressively relaxes when the cobalt ferrite content increases in the films.

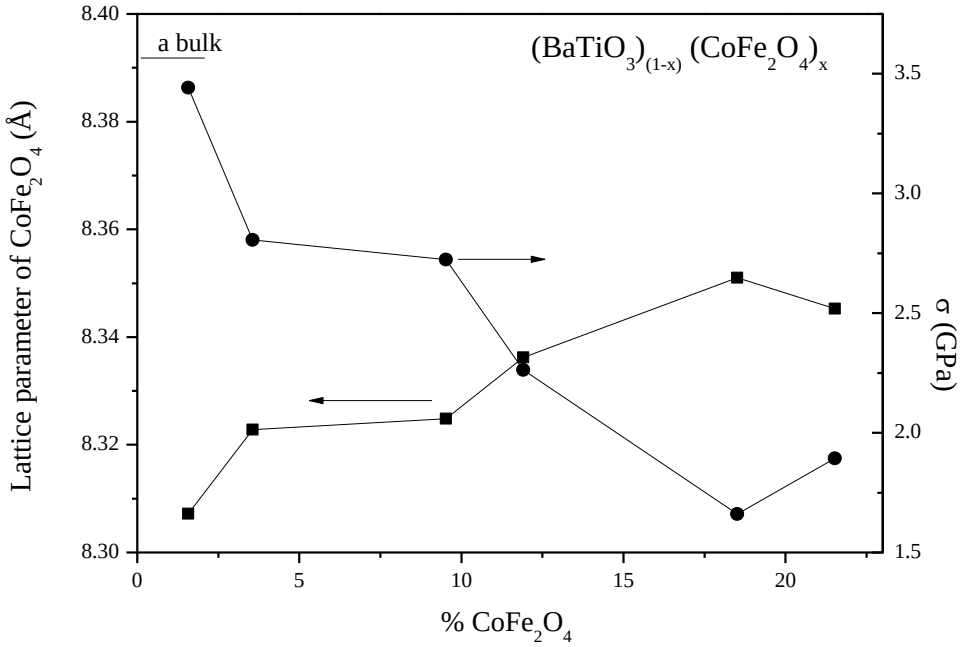

Figure 3: Left axis: $CoFe_2O_4$ lattice parameter obtained from (311). On the right side the in-plane biaxial stress on the $CoFe_2O_4$ grains estimated from those lattice parameters is plotted.

For $CoFe_2O_4$ grains, the determination of the magnitude of in-plane stress from lattice parameters obtained from interplanar distances of the (311) planes, is more complex. However, in order to have an estimation of their magnitude, the in-plane stress can be obtained from $\sigma = -\frac{Y}{2\alpha}\varepsilon$ [26] ($\sigma_1 = \sigma_2 = \sigma$) where the strain is $\varepsilon = (a_{CoFe2O4,film} - a_{CoFe2O4,bulk})/a_{CoFe2O4,bulk}$; $a_{CoFe2O4,film}$ is the lattice parameter determined from the (311) peak position, Y is the Young's modulus and α is the Poisson coefficient of the cobalt ferrite ($Y = 1.5\times10^2$ GPa, α=0.22 [28,29] at room temperature). The estimated stresses for the cobalt

ferrite phase are represented on the right axis of Figure 3. The $CoFe_2O_4$ grains are under an in-plane tensile stress (positive) that relaxes as the cobalt ferrite content increases from 3.4 GPa for x = 2% to 1.9 GPa for x = 22%.

The origin of the stresses on $BaTiO_3$ and $CoFe_2O_4$ phases on the films is related to the different thermal expansion coefficients. The thermal expansion coefficient for $CoFe_2O_4$, is 14.9×10^{-6} K^{-1} [30], while for silicon it is 2.6×10^{-6} K^{-1}. For $BaTiO_3$, its thermal expansion coefficients above and below the transition from the cubic to the tetragonal structure at T_{T-C} ~403 K, are 11.29×10^{-6} K^{-1} and 6.17×10^{-6} K^{-1} [31], respectively. During the $BaTiO_3$ laser ablation preparation step, the substrate, along with the cobalt ferrite layer, are heated to high temperatures, above T_{T-C}. As such, as the sample cools to room temperature, after $BaTiO_3$ deposition, the higher thermal expansion coefficient of $CoFe_2O_4$ relative to $BaTiO_3$ induces an in-plane compressive stress on $BaTiO_3$ due to a higher "shrinkage" of the $CoFe_2O_4$ phase along the $BaTiO_3$-$CoFe_2O_4$ interfaces. Correspondingly, an in-plane tensile stress on the cobalt-ferrite is imposed by the $BaTiO_3$ phase, while $BaTiO_3$ resists the induced compression due to the mechanical interactions between both phases. The increase of these in-plane compressive (tensile) stresses on $BaTiO_3$ ($CoFe_2O_4$), as the cobalt ferrite content increases on the films, is a consequence of the increase in interaction area between $BaTiO_3$ and $CoFe_2O_4$. Also, due to the lower thermal expansion coefficient of the substrate, relative to $CoFe_2O_4$, the same mechanism reinforces the tensile stress observed on $CoFe_2O_4$ grains.

3.2. Raman Spectroscopy

Due to the small size of the grains composing the films the diffraction peaks are broad and it is difficult, from the XRD results alone, to confirm which of the $BaTiO_3$ phases is present. In fact, as referred earlier, it is known that for small grain sizes the tetragonal distortion of the barium titanate crystallites is reduced due to the presence of a non-

ferroelectric grain boundary layer on the grains surface [25]. However, we observe a broadening of the (200) diffraction peak, with an increasing asymmetry of this peak towards higher angles suggesting the stabilization of a polar phase of $BaTiO_3$. To confirm the presence of this polar phase in the barium titanate layer and to further characterize its structure, Raman spectroscopy measurements have been performed. Raman spectroscopy yields phonon parameters reflecting the local crystal symmetry, allowing the detection of the presence of structural distortion of the grains unit cell.

Figure 4 shows the Raman spectra of the composite films, for cobalt ferrite concentrations in the range 4% - 22%. The spectra were deconvoluted using Gaussian line-shape functions to least-squares fit the observed bands.

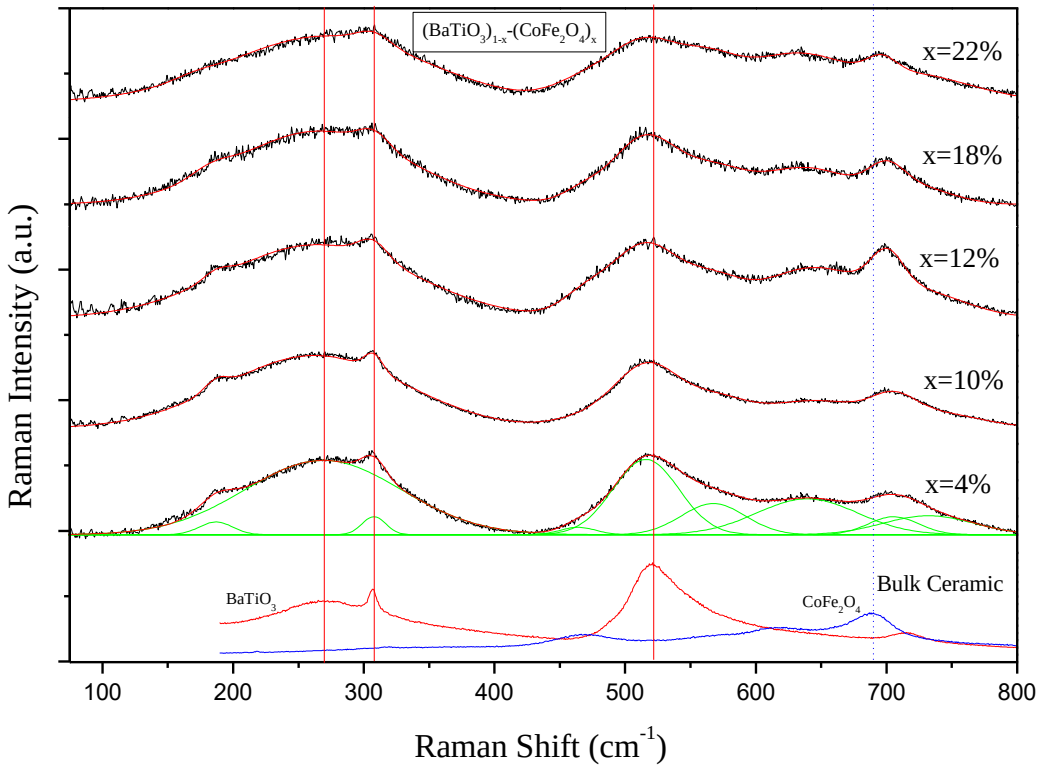

Figure 4: Raman spectra of the samples deposited with $CoFe_2O_4$ concentrations in the range 2%-22%, along with the corresponding fitting curves. The red lines show the position of main tetragonal/orthorhombic -$BaTiO_3$ Raman modes and the blue dotted line shows the position of cubic spinel CoFe2O4 mode at 695cm^{-1}.

Bulk cobalt ferrite has the inverse spinel structure. It has the space group Fd3m (O_g^7) and factor group analysis yields 39 vibrational modes, five of which are Raman active [32,33]. The active Raman modes are at 210 cm^{-1} (F_{2g}), 305 cm^{-1} (E_g), 466 cm^{-1} (F_{2g}), 577 cm^{-1} (F_{2g}) and 695 cm^{-1} (A_{1g}) [34]. Two main $CoFe_2O_4$ peaks are observed on the spectra. The peak seen near 700 cm^{-1} can be assigned to the A_{1g}, mode. It is shifted relative to the bulk due to the stress state of the cobalt ferrite nanoparticles in the films. As the $CoFe_2O_4$ concentration increases its position becomes nearer to the bulk value reflecting the relaxation of the stress on the cobalt ferrite, as already observed from the XRD results. Additionally, a small band (shoulder) appears near 470 cm^{-1} (for higher ferrite concentrations) and it can be assigned to an F_{2g} mode.

The cubic (paraelectric) phase of $BaTiO_3$ has a Pm3m (O_h) crystal symmetry, which, theoretically, does not have Raman active modes [35]. However, distortions to the perfect cubic cell, induced by disorder on the Ti positions or due to external stresses over the grains, can occur and broad peaks at around 250cm^{-1} and 520cm^{-1} have been observed on polycrystalline powders [16]. For the tetragonal phase (P4mm symmetry) fifteen modes are predicted: $3[A_1(TO)+A_1(LO)]+B_1+4[E(TO)+E(LO)]$. On the spectra of Figure 4, the main characteristic modes of tetragonal-$BaTiO_3$ are observed. They are at ~260 cm^{-1} (A_1(TO) mode), ~307 cm^{-1} (B1, E(TO+LO) modes) and ~516 cm^{-1} (E(TO)+A_1(TO) modes) [16].

The characteristic Raman bands of the $BaTiO_3$ orthorhombic phase are similar to the ones for the tetragonal phase, with differences on the 180 cm^{-1} region, where a peak appears on the orthorhombic phase, instead of a dip characteristic from the anharmonic coupling between the three A_1(TO) phonons typically observed on the tetragonal phase [16,35]. It is known that grain sizes and stresses can lead to a diffuse character of the tetragonal-orthorhombic phase transition, so that a coexistence of tetragonal and orthorhombic phases can occur at room temperature [13,14,18]. In this respect, the Raman peak observed near 180

cm^{-1} on the spectra of figure 4 indicates the presence of the orthorhombic phase at room temperature, coexisting with the tetragonal one, in the samples.

In Figure 5 the relative height between the (B1, E(TO+LO) (~307cm^{-1}) and E(TO)+A_1(TO) (~520cm^{-1}) $BaTiO_3$ modes is represented as a function of the $BaTiO_3$ grain size.

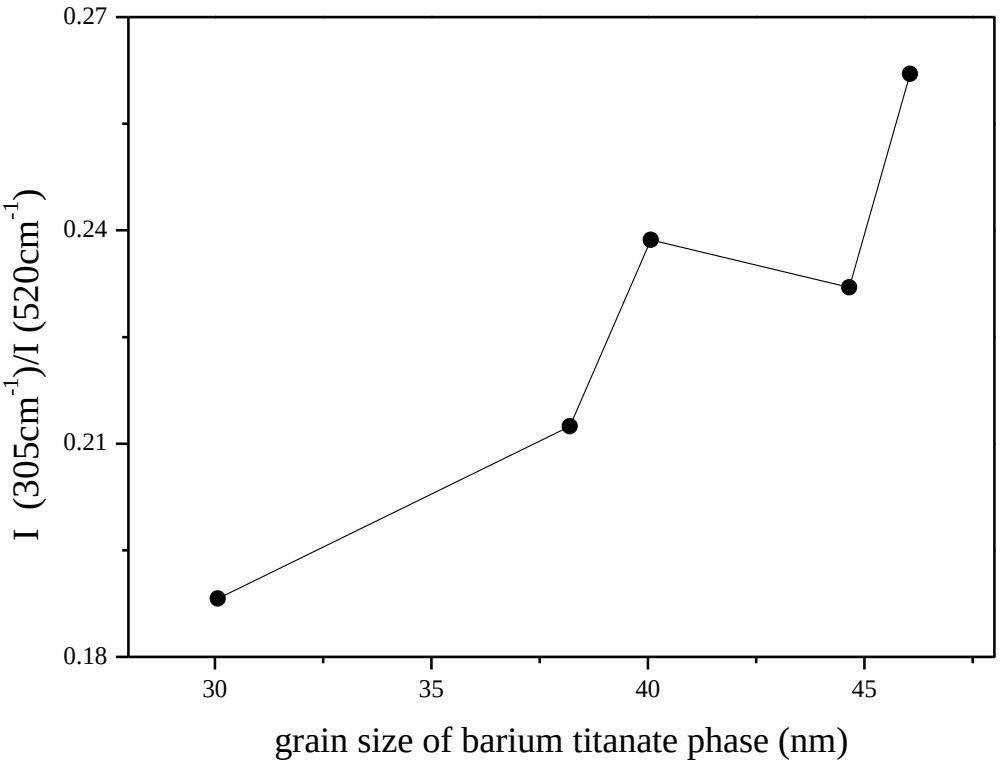

Figure 5: Relative intensity of $BaTiO^3$ (B1, E(TO+LO)) mode (at ~305cm^{-1}) relative to the E(TO)+A1(TO) mode (near 520cm^{-1}), as a function of the $BaTiO_3$ grain size.

The relative height of the 307cm^{-1} mode decreases when the corresponding $BaTiO_3$ grain size decreases. Since the 307cm^{-1} mode is characteristic of the polar (tetragonal, orthorhombic) phases of $BaTiO_3$ and does not exist in the cubic one, the observed increase of the relative intensity with increasing grain size is related with an increase of the polar distortion on the larger $BaTiO_3$ grains [16] and evidences the grain size dependence of the polar properties of $BaTiO_3$.

3.3. Temperature and frequency dependence of the dielectric permittivity

The $BaTiO_3$ grains on the films have grains sizes between 35-45nm and are under in-plane compressive stress. The $BaTiO_3$ phase stabilization depends critically on grain sizes and mechanical stresses, and the Raman spectroscopy results indicate the coexistence of orthorhombic and tetragonal phases at room temperature. In order to study the temperature dependent $BaTiO_3$ phase stabilization in these structures, the dielectric permittivity (ε') and loss tangent (*tan(δ)*) were measured for temperatures between 295K and 435K. Their corresponding results are shown on Figure 6.

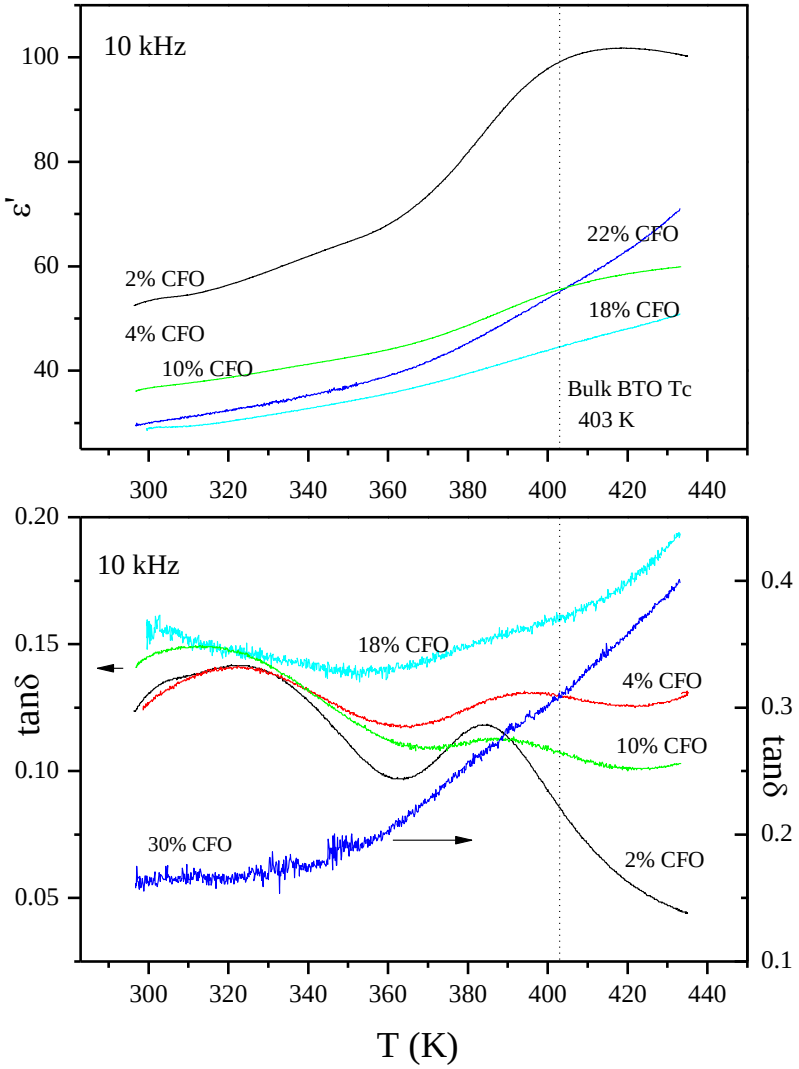

Figure 6: Temperature dependence of dielectric permittivity and loss tangent (ε' and *tan* (δ)), measured at 10 kHz. The dotted line shows the transition temperature (T_{T-C}) for the bulk material.

For cobalt ferrite contents of 2%, 4% and 10%, broad peaks are clearly identified for temperatures near 320K and 380K, particularly in the *tan(δ)* results (fig. 6). The peaks observed near 380K are ascribed to the $BaTiO_3$ tetragonal-cubic (T_{T-C}) phase transition, that in the bulk has been reported at ~403K [17]. For the samples with x=18% and x=22%, the permittivity is substantially broadened near T_{T-C} and the tetragonal-cubic phase transition is not so clearly observed. This is due to the increased contribution from the $CoFe_2O_4$ phase, that with a higher permittivity and loss tangent, particularly above T = 350K, obscures the $BaTiO_3$ contribution. The origin of the peaks observed at ~320K will be discussed later.

Shifts for lower temperatures of the tetragonal-cubic phase transitions (T_{T-C}), relative to the bulk, are observed, as shown in Figure 7. This behavior has been extensively reported in the literature [13,24,36], and particularly in thin films it is still a subject of debate, with several mechanisms proposed in order to explain the T_{T-C} shifts [36-38]. In this respect, its origin can be discussed in terms of the referred core-shell structure of $BaTiO_3$ grains, where grains are composed by a tetragonal core and a surface cubic layer. In order to describe the phase transition in this structure, the Ginzburg-Landau-Devonshire theory can be applied to inhomogeneous ferroelectrics, where a gradient and a surface term are added to Landau expression for a ferroelectric [39]:

$$F = \int \left[\frac{1}{2} A(T - T_{0\infty}) P^2 + \frac{1}{4} BP^4 + \frac{1}{2} D(\nabla P)^2 \right] dV + \int \frac{1}{2} D\delta^{-1} P^2 dS \qquad (3)$$

The volume and the surface integrals give the free energy of the grain interior and of the grain surface, $T_{0\infty}$ is the Curie-Weiss temperature of a bulk crystal, P the polarization, and *A*, *B*, *D* and δ are material constants. δ is the extrapolation length, which phenomenologically describes the difference between the surface and the bulk behavior of the polarization. Assuming spherical particles, with diameter *d*, omitting the gradient term, and with the appropriate boundary conditions, the size dependence of T_{T-C} becomes [39]:

$$T_{T-C} = -\frac{6D}{\delta A(d-2l)} + T_{T-C\infty} \qquad (4)$$

where the polarization is considered to change only along the grain radius. Also, a term *l* was subtracted to the grain size, in order to account for the contribution of the surface cubic layer of the grains [25].

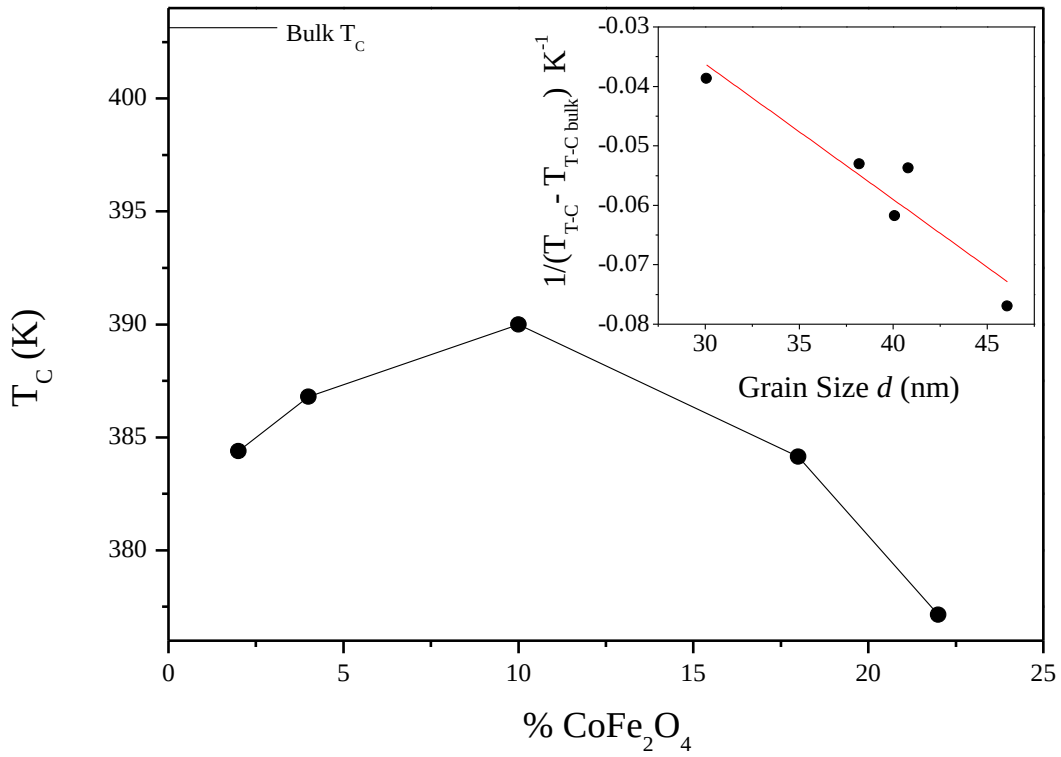

Figure 7: Tetragonal-cubic transition temperature as a function of the $CoFe_2O_4$ content in the samples. In the inserted graphic $\frac{1}{T_{T-C} - T_{T-C\infty}}$ is plotted as a function of $BaTiO_3$ grain size (dots). The line is the fit made with equation 4..

In the inset of Figure 7, $\frac{1}{T_{T-C} - T_{T-C\infty}}$ is plotted as a function of the $BaTiO_3$ grain size *d*, with $T_{T-C\infty}$ = 403 K. In the figure, the solid line is a fit to the experimental curve, made using equation 4 and the obtained fitting parameters are: $l = 7nm$ and $\frac{6D}{\delta A} = 4.39 \cdot 10^{-7}\, mK^{-1}$. The obtained value for the thickness of the surface cubic layer (*l*) is close to the estimated 10nm-15nm range for the reported thickness of the surface layer on the composite structure of

$BaTiO_3$ nanoparticles [25]. On the other hand, values of $A = 6.66\times10^5\ mF^{-1}K^{-1}$ and $D = 4.5\times10^{-9}\ m^3F^{-1}$ were reported and adopted by several authors [40,41]. From these values δ was estimated from the fit as $\delta = 93nm$, similar to the value of $\delta = 88nm$, previously reported from X-ray diffraction measurements [42]. The good agreement between the obtained fit parameters and previously reported ones on similar structures shows that, here, the $BaTiO_3$ grain size and its grains composite structure is determinant to the shifts of T_{T-C} to lower temperature.

As for the peaks observed near 320K at 10kHz, their behavior and, in particular, their frequency dependence is different. Figure 8 presents the dielectric constant and the loss tangent as a function of temperature, for x=4%, obtained for frequencies between 1kHz and 100kHz.

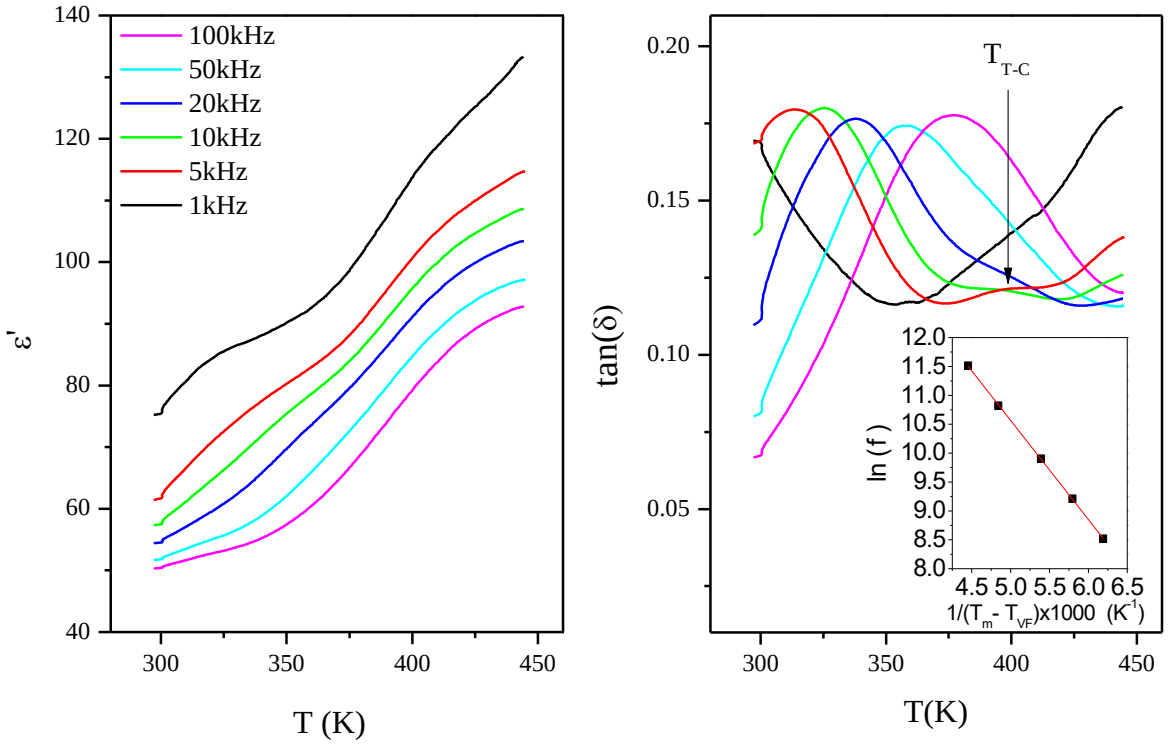

Figure 8: Temperature dependence of dielectric permittivity and loss tangent (ε' and *tan* (δ)), measured for frequencies between 1kHz – 100kHz for the sample with x=4%. The inset shows the fit using the Vogel-Fulcher relation of equation 5.

The figure shows that although the peak associated to the tetragonal-cubic phase transition did not change its position for different frequencies, the peak observed at 320K is broad and moves to higher temperatures as the frequency increases, with a dependence akin to a relaxor like behavior. In this respect, a strong frequency dispersion is observed (fig. 8) such that the relation between the temperature where the dielectric constant maximum appears (T_m) and the measuring frequency obeys the Vogel-Fulcher equation [43]:

$$f = f_0 \exp\left(\frac{-E_a}{k_b (T_m - T_{VF})}\right) \qquad (5)$$

where E_a and T_{VF} represent the activation energy and freezing temperature of the process. f_0 is a pre-exponential factor. The inset of Figure 8 shows the Vogel-Fulcher fit to the peak position for different frequencies. The obtained fitting parameters are $E_a = 0.15$ eV and $T_{VF} = 151.4$ K.

This type of relaxor-like behavior associated to a loss tangent peak near 320K has been reported before for epitaxial (Ba,Sr)TiO_3 films [44]. It was attributed to a frustrated phase transition between the tetragonal and orthorhombic phases, where the two phases coexist forming polar nanoclusters with different orientation of polarization. In bulk $BaTiO_3$, the transition between orthorhombic and tetragonal phases occurs at 280K. However, here, signs of the coexistence of tetragonal and orthorhombic phases at room temperature were observed by Raman spectroscopy. Thus, the combination of mechanical stresses and grain size effects on $BaTiO_3$ grains, arising from the mixed connectivity of the samples, lead to a frustrated orthorhombic-tetragonal phase transition and are the origin of the frequency dispersion behavior of the dielectric permittivity observed in the films near room temperature.

.

Conclusions

Nanostructured films composed by $CoFe_2O_4$ grains covered by a laser ablated $BaTiO_3$ layer were prepared with different cobalt ferrite concentrations. Their structure presented a combination of $BaTiO_3$, where its tetragonal and orthorhombic phases coexist at room temperature, and $CoFe_2O_4$ with the cubic spinel structure. The cobalt ferrite nanograins were under in-plane tensile stress, while the $BaTiO_3$ phase was under in-plane compressive stress.

In the dielectric permittivity and loss tangent results, two peaks were observed that were associated to the $BaTiO_3$ cubic-tetragonal and tetragonal-orthorhombic phase transitions. The cubic-tetragonal transition was shifted to lower temperatures due to the grains structure, with a polar core and cubic shell. On the other hand, a diffuse tetragonal-orthorhombic phase transition, near room temperature, was observed, associated with strong frequency dispersion similar to a relaxor-like behavior. This behavior was ascribed to grain size effects and mechanical stresses in the films, due to their mixed connectivity structure. They led to the formation of polar nanoclusters with random orientations of polarization, which induced a frustrated phase transition between the tetragonal and orthorhombic phases of barium titanate in the films.

Acknowledgements

This work has been supported by Fundação para a Ciência e Tecnologia (FCT) and FEDER, through the projects PTDC/CTM/099415/2008 and PTDC/CTM-NAN/115125/2009 and by QREN-ON2-O Novo Norte, through the project Operação Norte-070124-FEDER-000070.

References

[1] J. F. Scott, J. Mater. Chem., 22, 4567 (2012)

[2] J. Ma, J. Hu, Z. Li, C-W. Nan, Adv. Mater., 23, 1062–1087 (2011)

[3] L. Martin, Y.-H. Chuc, R. Ramesh, Mat. Sci. Eng. R, 68, 89 (2010).

[4] C. Nan, M. I. Bichurin, S. Dong, D. Viehland, G. Srinivasan, J. Appl. Phys., 103, 031101 (2008).

[5] H. Béa, M. Gajek, M. Bibes, A. Barthélémy, J. Phys.: Condens. Matter, 20, 434221 (2008).

[6] C.A.F. Vaz, J. Phys.: Condens. Matter, 24, 333201 (2012)

[7] H. Zheng, J. Wang, S. Lofland, M. Ma, L. Mohaddes-Ardabili, T. Zhao, L. Salamanca-Riba, S. Shinde, S. Ogale, F. Bai, D. Viehland, Y. Jia, D. Schlom, M. Wutting, A. Roytburd and R. Ramesh, Science, 303, 661-663 (2004).

[8] I. Levin, J. Li, J. lutsker, A. Roytburd, Adv. Mater., 18, 2044 (2006).

[9] H. Zheng, F. Straub, Q. Zhan, P. Yang, W. Hsieh, F. Zavaliche, Y. Chu, U. Dahmen and R. Ramesh, Adv. Mater., 18, 2747 (2006).

[10] C-W Nan, G. Liu, Y. Lin, Phys. Rev. Lett., 94, 197203 (2005)

[11] Y. Wu, J. Wan, C. Huang, Y. Weng, S. Zhao, J. Liu and G. Wang, Appl. Phys. Lett., 93, 192915 (2008).

[12] J. Barbosa, M. Pereira, C. Moura, J. Mendes, B. Almeida, Ferroelectrics, 421, 66 (2011).

[13] S. Lin, T. Lü, C. Jin, X. Wang, Phys. Rev. B, 74, 134115 (2006).

[14] Y. Li, L. Chen, Appl. Phys. Lett., 88, 072905 (2006).

[15] G. Arlt, D. Hennings, G. D. With, J. Appl. Phys., 58, 1619-1625 (1985).

[16] Y. Shiratori, C. Pithan, J. Dornseiffer, R. Waser, J. Raman Spectrosc., 38, 1300 (2007).

[17] W. Zhong, D. Vanderbilt, K.M. Rabe, Phys. Rev. Lett., 73, 1861 (1994)

[18] V. Buscaglia, M.T. Buscaglia, M. Viviani, T. Ostapchuk, I. Gregora, J. Petzelt, L. Mitoseriu, P. Nanni, A. Testino, R. Calderone, C. Harnagea, Z. Zhao, M. Nygren, J. Eur. Cer. Soc., 25, 3059 (2005).

[19] S. Aoyagi, Y. Kuroiwa, A. Sawada, H. Kawaji, T. Atake, J. Therm Anal. Calorim., 81, 627 (2005).

[20] X Wang, X Deng, H Wen, L Li, Appl. Phys. Lett., 89, 162902 (2006)

[21] T. Hoshina, H. Kakemoto, T. Tsurumi, S. Wada, M. Yashima, J. Appl. Phys., 99, 054311 (2006)

[22] B. Cullity, S. Stock, Elements of X-Ray Diffraction, Prentice Hall, (2001).

[23] Powder Diffraction File, Joint Committee on Powder Diffraction Standards, International Centre for Diffraction Data, Cards 5-626 ($BaTiOO_3$ - tetragonal), 22-1086 ($CoFe_2O_4$ - cubic spinel), (2004)

[24] M. H. Frey, D. Payne, Phys. Rev. B, 54, 3158 (1996).

[25] T. Hoshina, S. Wada, Y. Kuroiwa, T. Tsurumi, Appl. Phys. Let., 93, 192914 (2008)

[26] F. Rustichelli, J.J. Skrzypek (Eds), Innovative Technological Materials: Structural Properties by Neutron Scattering, Synchrotron Radiation and Modeling, Chap. 4, Springer-Verlag, Berlin, (2010)

[27] N. Pertsev, A. G. Zembil'gotov, R. Wazer, Phys. Solid State, 40, 2002 (1998).

[28] P.D. Thang, G. Rijnders, D.H.A. Blank, J. Magn. Magn. Mater. 310, 2621 (2007)

[29] V.G. Patil a, Sagar E. Shirsathb, S.D. Morec, S.J. Shuklac, K.M. Jadhav, J. Alloys Compound, 488, 199–203 (2009)

[30] L. Iyengar, B. Prasad, B. Qadri, Curr. Sci., 42, 534 (1973).

[31] Y. He, Thermochimica Acta, 419, 135 (2004).

[32] T. Yu, Z. Shen, Y. Shi, J. Ding, J. Phys.: Condens. Matter, 14, L613 (2002).

[33] W. White, B. De Angelis, Spectrochim. Acta A, 23, 985 (1967).

[34] M. Foerster, I. Milko, D. Nico, M. Xavier, B. Mykhailo, F. Sánchez and J. Fontcuberta, Adv. Funct. Mater., 22, 4344, (2012).

[35] V. Venkateswaran, V. Naik, R. Naik, Phys. Rev. B, 58, 14256 (1998).

[36] S. Chattopadhyays, P. Ayyub, V. Palkar, M. Multani, Phys. Rev.B, 52, 13177 (1995).

[37] W. Shih, W. Shih, I. Aksay, Phys. Rev. B, 50, 15575 (1994).

[38] G. Rossetti Jr., L. Cross, K. Kushida, Appl. Phys. Lett., 59, 2524 (1991).

[39] W. L. Zhong, Y. Wang, P. Zhang, B. Qu, Phys. Rev. B, 50, 698 (1994).

[40] H. Cao, T. Wu, W. Dong, Z. Li, Phys. Stat. Sol. (b), 238, 213 (2003).

[41] X. Wang, C. Wang, W. Zhong, D. Tilley, Solid State Commu., 121, 111 (2002).

[42] K. Ishikawa, T. Uemori, Phys. Rev. B, 60, 11841 (1999).

[43] S. Singh, S.P. Singh, D. Pandey, J. Appl. Phys., 103, 016107 (2008).

[44] M. Tyunina, J. Levoska, Phys. Rev. B, 70, 132105 (2004).